Materials Research Express

Biocompatible superparamagnetic carriers of chondroitin sulfate

To cite this article before publication: Luis M. R. Rivera *et al* 2019 *Mater. Res. Express* in press https://doi.org/10.1088/2053-1591/ab0950

Biocompatible superparamagnetic carriers of chondroitin sulfate

Luis M. R. Rivera[a,b], Leonardo G. Paterno[c], Natalia L. Chaves[b], Danijela Gregurec[d], Sônia N. Báo[b], Sergio E. Moya[d], Menka Jain[e], Ricardo B. Azevedo[b], Paulo C. Morais[a], Maria A. G. Soler[a]

[a] Instituto de Fisica, Universidade de Brasilia, Brasilia DF 70910-900, Brazil
[b] Instituto de Ciências Biológicas, Universidade de Brasilia, Brasilia DF 70910-900, Brazil
[c] Instituto de Quimica, Universidade de Brasilia, Brasilia DF 70910-900, Brazil
[d] Soft Matter Nanotechnology Laboratory, CIC biomaGUNE, Guipuzkoa 20009, Spain
[e] Department of Physics and Institute of Materials Science, University of Connecticut, Storrs CT 06269, USA

Abstract

The present study reports on the fabrication, morphological and structural characterizations, magnetic and biological tests of a biocompatible superparamagnetic carrier comprising iron oxide nanoparticle (ION) surface-functionalized with chondroitin sulfate (ChS), labelled ION@ChS. The reported ION@ChS sample is produced by alkaline coprecipitation of Fe^{2+} and Fe^{3+} ions in aqueous media in the presence of ChS. Fourier Transform infrared, Raman and x-ray photoelectron spectroscopies provide evidences for coordination of the ChS molecule (mainly through sulfonic groups) onto the ION's surface. As a consequence of this structural feature, the ION@ChSs show superior colloidal stability in physiological media (DMEM). Transmission electron microscopy reveals that the ION@ChS are nearly spherical (mean diameter = 8.2 nm ± 0.1) and almost monodispersed (diameter dispersity = 0.11 ± 0.01), while dynamic light scattering and electrophoretic mobility measurements confirm the presence of ChS at the ION's surface, providing mean hydrodynamic diameter (~ 100 nm) and very high negative zeta potential (around -50 mV). Moreover, the ION@ChS is superparamagnetic at room temperature, with no coercivity or remanence. Cell viability tests performed by means of the MTT assay indicates that ION@ChS shows no cytotoxiciy effect ($p < 0.05$). Therefore, one can anticipate potential biotechnological applications of the ION@ChS sample for site-specific delivery of ChS as well as a contrast agent in magnetic resonance imaging.

Keywords: Chondroitin sulfate, iron oxide nanoparticle, glycosaminoglycan, superparamagnetism, nanocarriers.

1. Introduction

Superparamagnetic iron oxide nanoparticles (IONs) provide ideal and unique platforms for multifunctional diagnostic and therapeutic agents [1] as they group together superparamagnetism, biocompatibility, and easy surface functionalization [2-5]. The ION-based biocompatible platforms comprise a nanomagnetic core whose surface is dressed with bio-friendly molecules, the later meant to provide the core with multifunctionality [6]. Besides that, surface coating is also engineered to ensure the colloidal stability of IONs in suspension at pH and ionic strength of physiological media. Lastly, surface coatings should also be designed to suppress quick uptake by the reticuloendothelial system while delivered into the blood stream [7-9]. Thus, ION surface functionalization protocols are a key step for a successful technological and biomedical applications of IONs [10-13]. As it is well-known, high-resolution magnetic resonance imaging can be accomplished by magnetically tagging tumor cells with ION-based materials [14, 15]. Additionally, chemotherapeutic agents [16] can be attached onto surface-functionalized IONs, which can thus enable specific targeting and delivery by either applying magnetic field gradients following injection into the blood circulation near the tumor site or via biological recognition using bioactive molecules attached onto the IONs' surface [17-19]. Consequently, to foster IONs' bio-inspired technologies it is of high interest to improve surface coating protocols that can support further development of nanomaterials platforms for diagnostic and/or drug delivering. Polymers are commonly used as a coating to improve the biocompatibility, stability and bioavailability of the IONs. As an example, superparamagnetic IONs coated with PVA showed no cytotoxicity when compared to uncoated IONs [20]. Dextran coated IONs where stable in various biological media up to 8 days [21]. Moreover, a glycosaminoglycan, hyaluronic functionalized IONs, highly selective for human hepatocellular liver carcinoma cells, has been developed [22]. Another glycosaminoglycan of interest is chondroitin sulfate.

Chondroitin sulfate (ChS) is a glycosaminoglycan with a polymeric chain that consists of 1:1 disaccharide units of 1,4-D-glucuronic acid and 1,3-*N*-acetyl galactosamine sulfate at either the 4- (4-

ChS) or 6-position (6-ChS) of the *N*-acetyl galactosamine subunit. Usually, ChS exhibits molecular weight in the range of 20–50 $\times 10^3$ g$\times$mol^{-1} [23-25] and it is synthesized in the intracellular environment from glucose or glucosamine precursors [26] and can be secreted in cartilage by chondrocytes as a macromolecular complex into the extracellular matrix (ECM) or else remains localized at the cell surface. Moreover, the secreted ChS can bind to a core protein to produce highly absorbent proteoglicans, which is a major structure inside cartilage and acts as shock absorber. ChS and glucosamine have been introduced as "nutraceutical agents" for treatment of osteoarthritis [27]. Importantly, investigations have shown that ChS exhibits anti-inflammatory and immunomodulatory effects [28], chondroprotective activity [29] and accounts for cell adhesion regulation [23]. These properties have promoted ChS as a promising for the development of biomaterial for cartilage regeneration [30] and tissue engineering [31]. ChS has been associated with inorganic nanoparticles aiming at stabilization of the latter, as reductant agent and as drug delivery system. For instance, metal iron and gold nanoparticles were successfully produced with ChS acting as both reductant and stabilizing agent [32, 33]. ChS-coated ION have been produced for manifold purposes, for example in the investigation of redox reactions of nitrite ions at the nanoparticles' surface [34], for preparation of hollow microspheres [35], in studies on colloidal stability in a wide range of pHs and salt concentrations [36], and for controlled delivery of doxorubicin hydrochloride [16]. More recently, polymeric nanoparticles were studied, like ChS self-assembled nanoparticles loaded with docetaxel (DTX), which improved DTX biodistribution and decreased metastasis-promotion protein expression of melanoma [37]. ChS can also be used to produce hydrogels containing specific drugs, like loxoprofen loaded hydrogels with improved release [38].

In the human body, chondrocytes have an important role in cartilage maintenance. Due to the limited proliferation potential of chondrocytes and their catabolic response to pathological mediators, cartilage can spontaneously repair small damages. Additionally, the avascular nature of cartilage prevents immigration of regenerative cells [30] to the affected site. In this regard, ChS can be prescribed as part of the medical treatment although its efficacy should depend on the route of administration. In the present study, we report on a simple and effective method of synthesis to obtain a biocompatible ChS-coated ION

carrier for ChS site delivery. The as-fabricated ChS-nanocarrier represents a step forward in the delivery of ChS to damaged cartilage once it is designed for intra-articular injection, aiming the effective interiorization by the chondrocytes. Moreover, its effectiveness should be enhanced by application of an external gradient of magnetic field, thus improving site-localization. The synthesis protocol of the new ChS-nanocarrier consists on aqueous co-precipitation of ION in the presence of ChS (ION@ChS). In fact, the covalent interaction between ION and ChS that prevails in the ION@ChS sample is reflected in its superior colloidal stability at physiological conditions. Dynamic light scattering, transmission electron microscopy, Raman, Fourier transform infrared and x-ray photoelectron spectroscopies and magnetic measurements were carried out for structural characterization of bare and ChS-functionalized IONs samples. *In vitro* cytotoxicity of ChS-coated ION carriers against human dental pulp fibroblast cells was assessed by the MTT assay.

2. Materials and Methods

2.1. Materials

$FeCl_2{\cdot}4H_2O$, $FeCl_3{\cdot}6H_2O$, NaOH, HCl, chondroitin-4-sulfate (ChS) extracted from bovine trachea, Prussian blue and Nuclear Fast Red were all purchased from Sigma Aldrich (USA) and used as received. Dulbecco's Modified Eagle Medium (DMEM), PBS and MTT were acquired from Gibco Life Technologies Inc. (USA). All water used for synthesis and suspension preparations was provided by a Milli-Q water purification system (water resistivity: 18 $M\Omega{\times}cm^{-1}$).

2.2. Synthesis of colloidal samples

Samples were produced by precipitation of IONs from a mixture of 1:2::Fe2+:Fe3+ ions with aqueous solution of NaOH at room temperature (bare ION employed as control sample) or in the presence of ChS (sample ION@ChS). The employed route is schematically illustrated in Scheme 1. Actually, the

protocol for synthesizing the IONs is the same as the one described by Kang et al. [39] and reproduced elsewhere [40, 41]. In short, $FeCl_2 \cdot 4H_2O$ (25 mL, 0.30 mol×L^{-1}) and $FeCl_3 \cdot 6H_2O$ (25 mL, 0.60 mol×L^{-1}) aqueous solutions were mixed and slowly added to 150 mL of NaOH (2.0 mol×L^{-1}) and kept under mechanical stirring (2,000 rpm), at room temperature, for extra 30 min. A black precipitate (solid magnetite, Fe_3O_4 or simply ION) obtained at the end was isolated by centrifugation and washed several times with ultrapure water. A stock aqueous suspension of positively-charged ION (sample ION) was produced by dispersing the as-produced IONs into aqueous solution of perchloric acid (0.25 mol×L^{-1}) with mechanical stirring overnight. The suspension was then centrifuged for elimination of aggregates and adjusted to pH3 with perchloric acid solution, being from now on considered as control sample. The acidic medium provides protonation of the IONs' surface sites [42] and the resulting colloid is stabilized by repulsive electrostatic interaction. For preparation of the ION@ChS sample, an identical 1:2::Fe^{2+}:Fe^{3+} solution was prepared and mixed with ChS (0.1 g×L^{-1}), producing a clear solution after gentle magnetic stirring. Next, the as-prepared solution (Fe^{2+}/Fe^{3+} plus ChS) was slowly added to 750 mL of NaOH (1.5 mol×L^{-1}, pH 13) under mechanical stirring and kept under stirring for extra 30 min, at room temperature. The ION@ChS black precipitate was washed 3 times with ultrapure water and then suspended in ultrapure water (pH=5.5) using overnight mechanical stirring. The resulting colloid (magnetic fluid sample) was then centrifuged (2147 g, 10 minutes) to remove aggregates. The resulting ION@ChS colloidal suspension was dialyzed against ultrapure water for 24 h. The dialyzed suspension was adjusted to pH7.2. The final ION@ChS colloid changed color from black to dark brown after the dialysis step, suggesting partial oxidation of the as-precipitated IONs, from magnetite (Fe_3O_4) to maghemite (γ-Fe_2O_3). A small aliquot of each colloidal sample, i.e. ION and ION@ChS, was freeze-dried for 3 days in a vacuum chamber for further structural characterization in its solid, powder form. Dried samples were labeled s-ION and s-ION@ChS.

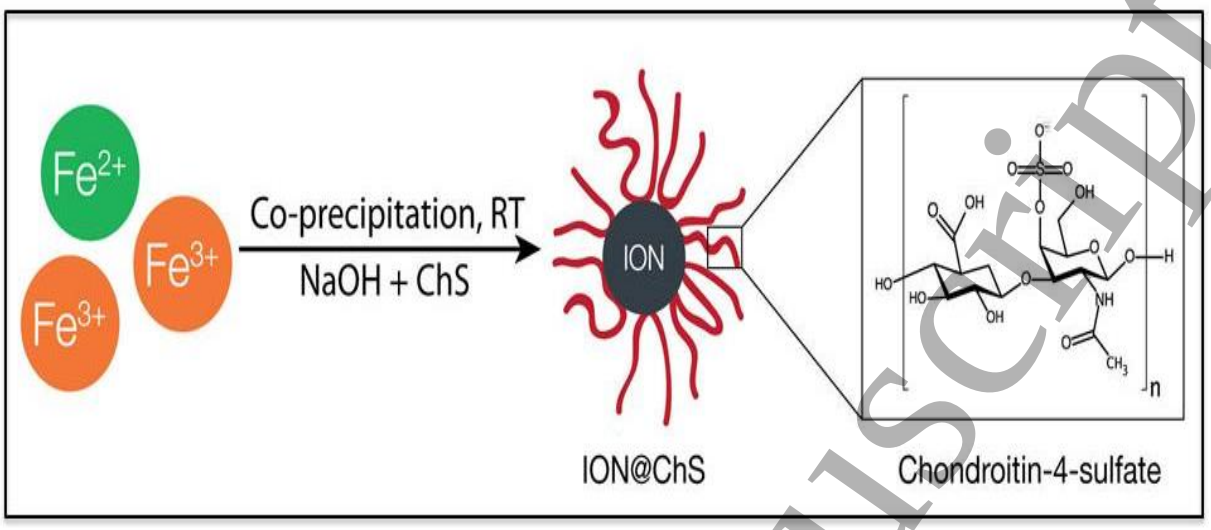

Scheme 1 – Illustration of the synthesis processes employed to produce the ION@ChS sample.

2.3. *Sample morphology and structural characterization*

Morphology, mean diameter size (D_{TEM}) and polydispersity index (σ) of the as-produced ION-based structures were assessed using transmission electron microscopy (TEM) images recorded in a JEOL JEM-1011 system. Additionally, mean hydrodynamic diameter (D_H), determined using number distribution, and zeta potential (ζ potential) of colloidal samples (ION and ION@ChS) were determined by Dynamic Light Scattering and electrophoretic mobility measurements using a Nano ZetaSizer Z90 instrument from Malvern. Structural features of dried samples (s-ION and s-ION@ChS) were assessed by micro Raman, Fourier transform-infrared (FT–IR) and x-ray photoelectron (XPS) spectroscopies. The employed micro Raman system was a commercial triple spectrometer (Horiba Scientific) equipped with a liquid N_2 cooled CCD detector. Spectra were recorded at room temperature while exciting the samples with an Argon ion laser (λ = 514 nm) operating at 0.25 mW. FT-IR measurements were carried out in a Vertex 70 spectrometer (Bruker Corporation, USA) in transmittance mode with samples dispersed in KBr pellets. Spectra were recorded in the range of 500 to 1800 cm^{-1} using the system's resolution set at 4 cm^{-1} while

performing 128 scans. XPS data were collected in a SPECS SAGE HR 100 system equipped with an AlKα source (non-monochromatic, operating at 12.5 kV and 300 W) and take-off angle of 90º with pressure set at ~10^{-8} Torr. Energy shift in the spectra was corrected by the C(1s) energy line at 284.7 eV. Detailed spectra for O(1s) and S(2p) was recorded with pass energy of 10 eV.

Room temperature magnetization measurements (field−dependent) of the samples were carried out in a Quantum Design vibrating sample magnetometer connected to an Evercool physical property measurement system. The contribution of ChS in the ION@ChS weight was removed out by measuring its content via thermogravimetric analysis (TGA), as described elsewhere [11]. TGA was also used to extract the ChS content in colloidal samples used in the biological assay. TGA curves (not shown) of powdered samples (~ 5mg) were acquired from 25 to 500 ºC at heating rate of 10 ºC min^{-1} with a DTG-60H Shimadzu thermo-analyzer under nitrogen atmosphere (30 mL×min^{-1}).

2.4. In vitro cytotoxicity assay

Human connective tissue cells harvested from dental pulp of normal teeth were maintained in primary culture [43]. Cells were cultured in Dulbecco's modified Eagle's medium (DMEM) supplemented with 10% fetal bovine serum (Gibco Life Technologies, USA) and 100 U×mL^{-1} penicillin plus 100 μg×mL^{-1} streptomycin (Gibco Life Technologies Inc., USA) in an incubator with 5% CO_2 and 80% humidity at 37 °C. The cytotoxicity assay was conducted with cells seeded at 3×10^3 cells/well in flat-bottomed 96-well plates in triplicates for 24 h. The MTT assay was conducted comprising three independent experiments. The medium was renewed and ChS solutions (0.0125% and 0.0250%, w/v) or colloidal ION@ChS (at same concentration of ChS) were added. Plates were incubated at 37 °C for 24, 48, and 72 h. Toxicity was determined by removing residual solutions, following PBS rinsing and culture medium reestablishment. Cytotoxicity was determined by 3-(4,5-dimethylthiazol-2-yl)-2,5-diphenyltetrazolium bromide (MTT) assay with cells incubated at different elapsed times. Cells were maintained with DMEM and MTT (5 mg×mL^{-1}, dissolved in PBS), and incubated at 37 °C in a CO_2

incubator for 2 h. The resulting solution was carefully removed and 100 μL of dimethyl sulfoxide was added in order to solubilize the as-produced violet formazan crystals. The solution's absorbance at 595 nm was measured in a 96-well spectrophotometer microplate reader (SpectraMax M2, Molecular Devices, USA). The recorded data were normalized to the control data (cells treated with PBS only). Statistical analysis (ANOVA two-way, $p<0.05$) was performed using the GraphPad Prism 5 software.

3. Results and Discussion

3.1. Characterization of the colloidal samples

The ChS coating onto the IONs' surface in the as-prepared colloidal suspension was confirmed by measuring the ζ potential. The ζ potential obtained for the stock acid ionic colloidal suspension (ION sample) was +19.7 mV, consistent with the positively charged surface originated from protonation of the hydroxyl surface groups [42, 44]. In addition, the ζ potential of the ION@ChS was –56.8 mV, attributed to the presence of deprotonated carboxyl and sulfate groups from ChS. The impressively high negative ζ potential value found in the ION@ChS explains its superior colloidal stability, typically achieved with ζ potential higher than ±30 mV. Moreover, the observed ζ potential value is also consistent with the presence of ChS onto the IONs' surface. Recorded D_H values were 50.7 nm and 105.7 nm for the ION and ION@ChS samples, respectively.

Morphology and diameter distribution of the ION@ChS sample were assessed by TEM. Fig. 1 shows the particle diameter histogram (vertical columns) and a typical TEM image (see inset). The TEM micrograph reveals mostly spherical nanoparticles with diameter distribution well-fitted by a log-normal distribution function (solid blue line), providing a mean particle diameter of D_{TEM} = 8.2 ± 0.1 nm and polydispersity index of σ = 0.11 ± 0.01 for the s-ION@ChS sample. From recorded TEM images (not shown) of the s-ION sample (control sample) the attained values of D_{TEM} and σ were 7.0 ± 0.1 nm and 0.27 ± 0.01, respectively.

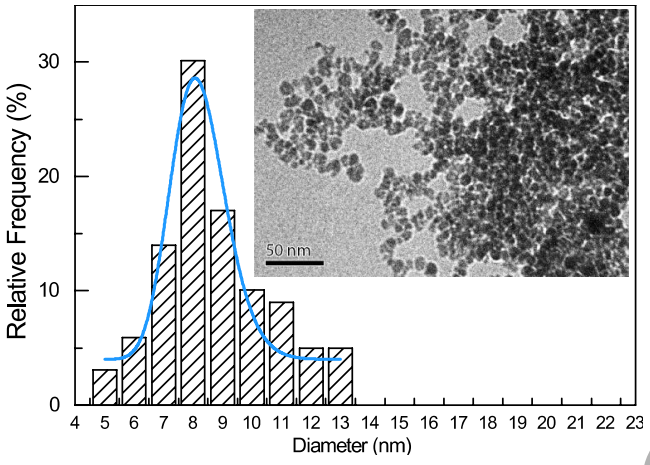

Fig. 1. Particle diameter distribution (vertical columns) curve-fitted with a log-normal distribution function (solid blue line) of the ION@ChS sample. The inset shows a typical TEM image (scale bar equals to 50 nm).

Fig. 2 displays the Raman spectrum of the s-ION@ChS sample at laser intensity of 0.25 mW. Lower laser power was used to avoid sample degradation under optical excitation [45]. Raman modes were identified in Fig. 2 (dashed blue lines) based on data available in the literature for the characteristic vibrational modes of the cubic spinel O_h^7 (Fd3m space group: T_{2g}^1 at 193 cm^{-1}, E_g at 306 cm^{-1}, T_{2g}^2 in the range of 450-490 cm^{-1}, T_{2g}^3 at 538 cm^{-1}, and A_{1g} at 668 cm^{-1}), describing normal modes of magnetite Fe–O tetrahedron and bands around 350, 500 and 700 cm^{-1} assigned to bulk maghemite [46]. The Raman fitting procedure employed Lorentzian-like components (dashed blue lines in Fig. 2) and reveals the presence of structures at 326, 535 and 668 cm^{-1} (s-ION@ChS sample), which were assigned to magnetite vibrational modes. Moreover, small bands associated with maghemite phase can also be identified at 371, 501 and 709 cm^{-1} (s-ION@ChS), which thus suggests that the IONs were partially oxidized and, therefore, they should be considered a mixture of magnetite and maghemite phases. The oxidation of IONs is expected once no care was taken to control oxygen during sample preparation.

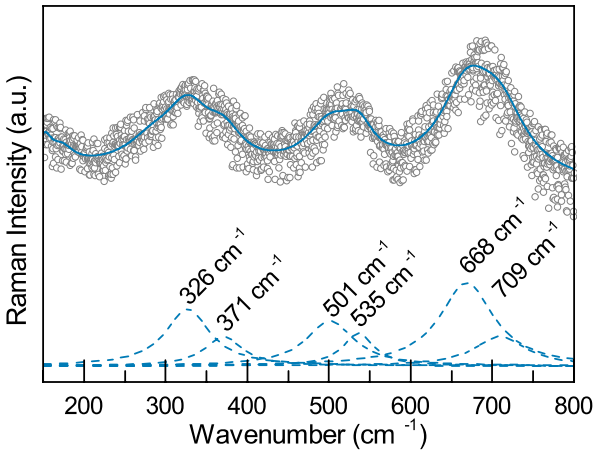

Fig. 2. Raman spectrum (open symbols) of the s-ION@ChS sample with Ar^+ laser intensity set at 0.25 mW. Deconvoluted components are shown in dashed blue lines.

In order to confirm the presence of ChS and investigate the way it is likely attached onto the IONs' surface, FT-IR analyses of the ChS and ION@ChS samples were performed. Peaks in the FT-IR spectrum of the ChS sample observed in Fig. 3 were assigned according to the literature [47, 48]. For example, axial SO_3^- stretching is found at 858 and 730 cm^{-1}, while the shoulder centered at 987 cm^{-1} is assigned to C–O–S stretching of the sulfate group present in carbon 4 of GalNAc [48]. The symmetrical and asymmetrical S=O stretching of sulfate group bonds are observed at 1065 and 1253 cm^{-1}, respectively [47, 48]. Moreover, the symmetrical and asymmetrical stretching of the C–O–C bond are observed at 1035 cm^{-1} [47] and 1124 cm^{-1} [48], respectively. The vibrations regarding the carboxylate group are observed at 1418 and 1652 cm^{-1}, being the former assigned to the symmetrical stretching [47] and the latter to the asymmetrical stretching [48]. The in-plane amide bending mode can be observed as a shoulder centered around 1568 cm^{-1}[48]. The FT-IR spectrum of the s-ION@ChS sample (Fig. 3) is composed by the main bands found in the ChS sample, thus confirming the presence of ChS onto the IONs' surface. Moreover, the spectrum of the s-ION@ChS sample shows a systematic red-shift of most of the bands as well the intensity decrease of the symmetrical C=O stretching mode, which strongly suggests the interaction of the ChS molecule with the ION's surface via this functional group (Table 1). In particular, the remarkable band-shift of both the carboxylate asymmetrical stretching ($\Delta\tilde{\nu}_a(COO^-)$ = –18 cm^{-1}) and the sulfate ($\Delta\tilde{\nu}_s(S{=}O)$ = –11 cm^{-1} and $\Delta\tilde{\nu}_a(S{=}O)$ = +10 cm^{-1}) is possibly due to coordination

of these two groups to iron(II) at the ION's surface [49]. Furthermore, the wide band at 580 cm^{-1} is attributed to the Fe-O bond from the magnetite phase [50, 51].

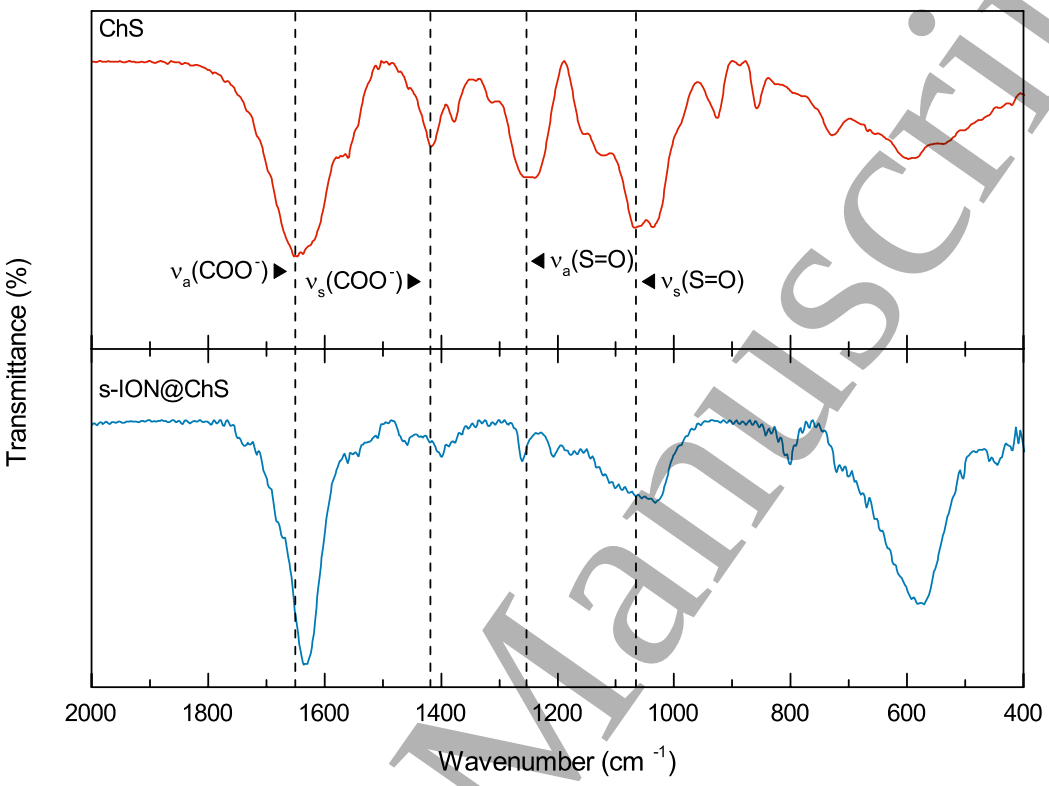

Fig. 3. FT-IR spectra of the ChS (upper panel) and s-ION@ChS (lower panel) samples. Vertical lines are guides for observation of peak positions based on ChS.

Table 1 – Selected FT-IR peaks (Fig. 3) of the ChS and s-ION@ChS samples with their respective assignments and peakshifts.

Sample	ChS	s-ION@ChS	
Assignment	$\tilde{\nu}$ (cm^{-1})	$\tilde{\nu}$ (cm^{-1})	$\Delta\tilde{\nu}$ (cm^{-1})
$\nu_{ax}(SO_3^-)$	730	714	–16
	858	806	–52
$\nu_s(S=O)$	1079	1068	–11
$\nu_a(S=O)$	1248	1258	+10
$\nu_s(COO^-)$	1418	1399	–19
$\nu_a(COO^-)$	1650	1632	–18

XPS analyses in the O(1s) and S(2p) regions were performed to further investigate the interaction between ChS and the IONs' surface (Fig. 4a). The Fe-O peak in both s-ION and s-ION@ChS samples is observed around 530 eV. Analysis of the S(2p) region (Fig. 4b), however, shows a metallic Fe(SO_4) peak in the s-ION@ChS sample (169 eV). Moreover, in the C(1s) region, peaks assigned to C-O and C=O show a small shift to higher energy, when comparing the s-ION@ChS sample with the ChS molecule (data not shown). The presence of these peaks corroborates the FT-IR data and indicates coordination of the ChS sulfate group onto the ION's surface iron.

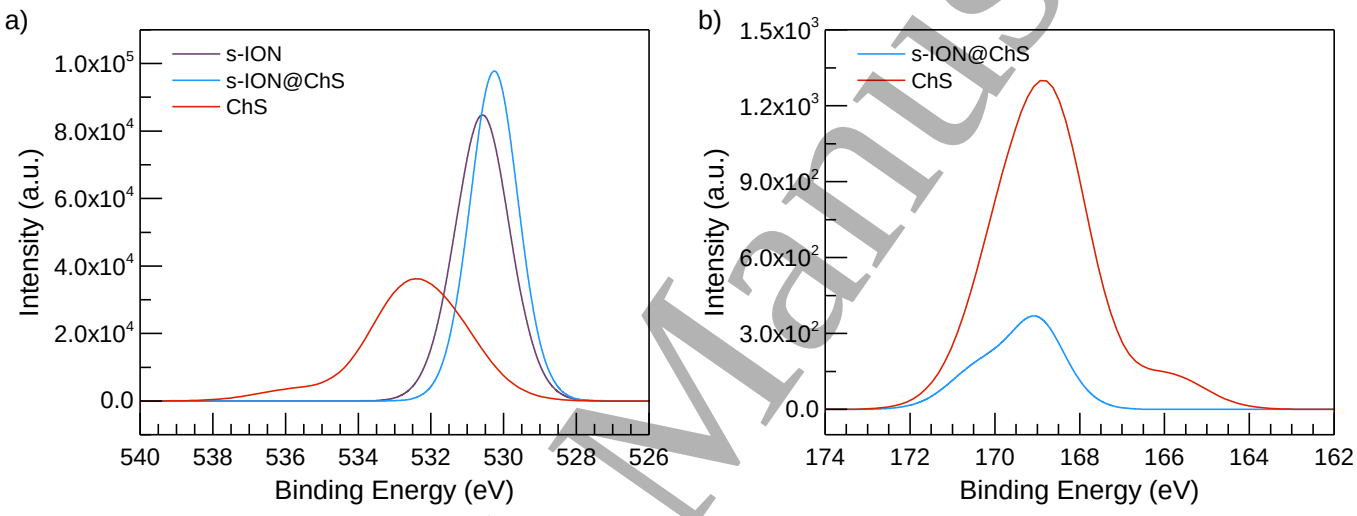

Fig. 4. XPS spectra in the (a) O(1s) region for the s-ION, s-ION@ChS and ChS samples and (b) S(2p) region in the s-ION@ChS and ChS samples.

The magnetic behavior (magnetization versus applied field) of the s-ION@ChS sample was measured in the field range of ±10 kOe, at 5 K and 300 K, as shown in Fig. 5. The inset of Fig. 5 shows the zoomed hysteresis loops in the ±0.5 kOe window registered at 5 K and 300 K. It is worth noticing from the inset of Fig. 5 that the s-ION@ChS sample exhibits neither remnant magnetization (M_R) nor coercivity (H_C) at 300 K, as expected for IONs in the assessed size range (D_{TEM} = 8.2 ± 0.1 nm). The saturation magnetization (M_S) was estimated by plotting the magnetization versus the reciprocal of the applied field [52]. The obtained values for M_S were 58 emu/g (5 K) and 53 emu/g (300 K). Both M_S values are smaller than that reported value for bulk maghemite at 4 K (M_S = 85 emu/g), however, are greater than for superparamagnetic IONs of similar size coated with dextran [53, 54]. The decrease of the

saturation magnetization is expected for nanosized magnetic materials, likely due to surface spin canting and disorder associated with broken bonds and frustration of long-range exchange interaction due to the lack of translational symmetry [55, 56].

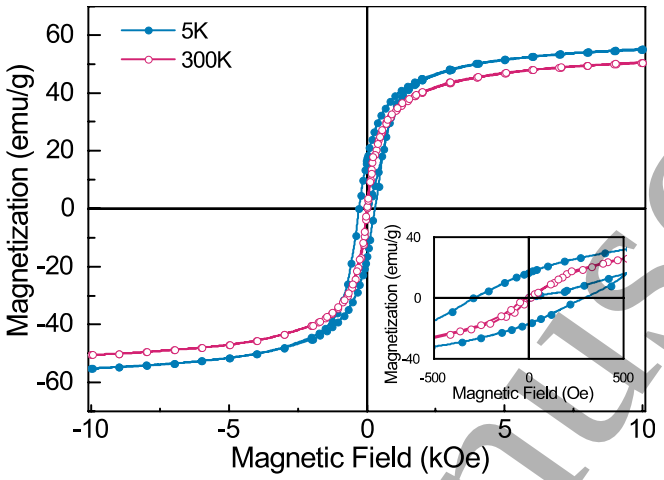

Fig. 5. Magnetization versus magnetic field curve of s-ION@ChS at 5 K and 300 K. The inset shows a magnified window of the *M*×*H* curves in the ±0.5 kOe range, showing the superparamegnetic behavior at 300 K.

3.2. Cell viability test

The cell viability measured at 24, 48, and 72 h after incubation of cells with only PBS (control), pure ChS and colloidal ION@ChS at different ChS concentrations (0.0250 % and 0.0125 % (w/v)) are displayed in Fog. 6a and Fig. 6b, respectively. Despite no statistical significance ($p < 0.05$) when compared with the control group, no cytotoxic effects were observed from the performed assay.

Due to the natural biocompatibility of the ChS one could expect high cell viability. It was found in the literature, that ChS promote cell proliferation in human fibroblasts [57] and chondrocytes [58]. Moreover, the small increase in cell viability over time when cells were treated with ION@ChS, observed in Fig. 6, may indicate a modulation of the release of ChS, as its coordination with the ION surface must be cleaved before to be catabolized. Moreover, the catabolism of chondroitin sulfate has been investigated [59] showing that ChS degradation occurs predominantly in lysosomes after endocytosis involving a large quantity of enzymes. Its depolymerization begins with endo-type hydrolases and the resulting

oligosaccharides are consequentially cleaved by exo-type glycosidases and sulfatases (herein, GALNS: N-acetylgalactosamine-4-sulfate sulfatase), which liberates monosaccharide moieties. The catabolism of ChS normally consists in 9 steps, resulting in the monosaccharides glucoronic acid and *N*-acetil-galactosamine and inorganic sulfate. Although as ChS is abundantly present in cartilage, it is widely distributed and therefore most cells are able to catabolize it.

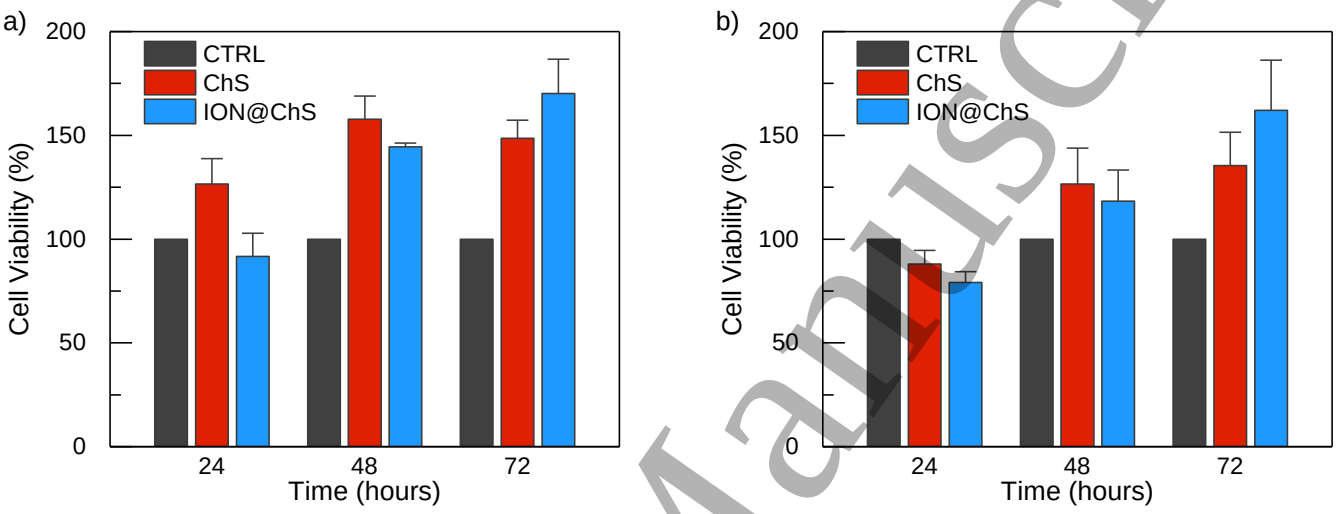

Fig. 6. Cell viability assay after 24, 48 and 72 h of treatment with ChS in concentration of (a) 0.0125% (w/v) and (b) 0.0250% (w/v).

4. Conclusion

We have shown the successful one-pot synthesis of biocompatible nanocarriers with room-temperature superparamagnetic properties comprising an iron oxide nanoparticle (ION) core, with mean diameter around 8 nm (diameter dispersity around 0.1), surface-functionalized with chondroitin sulfate (ChS). According to different spectroscopy techniques (FT-IR, Raman, and XPS) and complemented with zeta potential and dynamic light scattering measurements, ChS is attached to ION by complexation of its carboxylate and sulfate groups to surface iron atoms (II and III) during alkaline coprecipitation. This would contribute for the nanoparticulated system to reach the target tissue. Therefore, the herein produced nanocomposite could diffuse through the cartilage and enter the lacunae where it would be interiorized by

the chondrocytes. Additionally, the ION@ChS exhibits typical room-temperature superparamagnetic behavior, showing neither hysteresis nor remanence, with relatively high saturation magnetization of 53 emu/g at 300 K (and 58 emu/g at 5 K). Moreover, *in vitro* assay shows that the ION@ChSs have no cytotoxic effect. In conclusion, the ION@ChS colloidal sample produced under the present synthetic route is highly promising for future biomedical applications as for instance in site-specific delivery of ChS in tissues and as a contrast agent in magnetic resonance imaging.

Acknowledgments

The financial support from the Brazilian agencies MCT-CNPq, FINEP, FAP-DF, FINATEC and CAPES is gratefully acknowledged. Support from the FP7-PEOPLE-HIGRAPHEN project (612704) is also acknowledged. We are grateful to Dr. M. J. Araújo Sales, Instituto de Quimica - Universidade de Brasília, for her support with TGA measurments. Also, Dr. O. R. Pires Júnior, Instituto de Ciências Biológicas - Universidade de Brasília, is acknowledged for his support with sample lyophilization.

References

1. Yoo D, Lee J-H, Shin T-H, Cheon J. Theranostic magnetic nanoparticles. Accounts of chemical research. 2011;44(10):863-74.

2. Bonder MJ, Huang Y, Hadjipanayism GC. Magnetic Nanoparticles. In: Sellmyer DJ, Skomski R, editors. Advanced Magnetic Nanostructures. New York, NY: Springer; 2006. p. 183-206.

3. Trahms L. Biomedical applications of magnetic nanoparticles. In: Odenbach S, editor. Colloidal Magnetic Fluids. Germany: Springer-Verlag Berlin Heidelberg; 2009. p. 328-58.

4. Soler MAG, Paterno LG. 6 - Magnetic Nanomaterials. In: Da Róz AL, Ferreira M, de Lima Leite F, Oliveira ON, editors. Nanostructures: El Sevier; 2017. p. 147-86.

5. Vassiliou JK, Mehrotra V, Russell MW, Giannelis EP, McMichael R, Shull R, et al. Magnetic and optical properties of γ - Fe2O3 nanocrystals. Journal of applied physics. 1993;73(10):5109-16.

6. Guo X, Wu Z, Li W, Wang Z, Li Q, Kong F, et al. Appropriate Size of Magnetic Nanoparticles for Various Bioapplications in Cancer Diagnostics and Therapy. ACS applied materials & interfaces. 2016;8(5):3092-106.

7. Begin-Colin S, Felder-Flesch D. Strategies for functionalisation of magnetic nanoparticles for biological targets. In: Thanh NTK, editor. Magnetic Nanoparticles: From Fabrication to Clinical Applications. Boca Raton, FL, USA: CRC Press Taylor & Francis Group; 2012. p. 151-91.

8. Soler MAG, Lima ECD, Nunes ES, Silva FLR, Oliveira AC, Azevedo RB, et al. Spectroscopic Study of Maghemite Nanoparticles Surface-Grafted with DMSA. J Phys Chem A. 2011;115(6):1003-8.

9. Galli M, Guerrini A, Cauteruccio S, Thakare P, Dova D, Orsini F, et al. Superparamagnetic iron oxide nanoparticles functionalized by peptide nucleic acids. RSC Advances. 2017;7(25):15500-12.

10. Ling D, Lee N, Hyeon T. Chemical synthesis and assembly of uniformly sized iron oxide nanoparticles for medical applications. Accounts of chemical research. 2015;48(5):1276-85.

11. Viali WR, Alcantara GB, Sartoratto PPC, Soler MAG, Mosiniewicz-Szablewska E, Andrzejewski B, et al. Investigation of the Molecular Surface Coating on the Stability of Insulating Magnetic Oils. J Phys Chem C. 2010;114(1):179-88.

12. Philip J, Laskar JM. Optical properties and applications of ferrofluids—a review. Journal of nanofluids. 2012;1(1):3-20.

13. Marradi M, Chiodo F, Garcia I, Penadés S. Glyconanoparticles as multifunctional and multimodal carbohydrate systems. Chemical Society Reviews. 2013;42(11):4728-45.

14. Gao Z, Ma T, Zhao E, Docter D, Yang W, Stauber RH, et al. Small is smarter: nano MRI contrast agents–advantages and recent achievements. Small. 2016;12(5):556-76.

15. Wang J, Zhang B, Wang L, Wang M, Gao F. One-pot synthesis of water-soluble superparamagnetic iron oxide nanoparticles and their MRI contrast effects in the mouse brains. Materials Science and Engineering: C. 2015;48:416-23.

16. Mallick N, Anwar M, Asfer M, Mehdi SH, Rizvi MMA, Panda AK, et al. Chondroitin sulfate-capped super-paramagnetic iron oxide nanoparticles as potential carriers of doxorubicin hydrochloride. Carbohyd Polym. 2016;151:546-56.

17. Pankhurst Q, Thanh N, Jones S, Dobson J. Progress in applications of magnetic nanoparticles in biomedicine. Journal of Physics D: Applied Physics. 2009;42(22):224001.

18. Hadjipanayis CG, Machaidze R, Kaluzova M, Wang L, Schuette AJ, Chen H, et al. EGFRvIII antibody–conjugated iron oxide nanoparticles for magnetic resonance imaging–guided convection-enhanced delivery and targeted therapy of glioblastoma. Cancer research. 2010;70(15):6303-12.

19. Korrapati PS, Karthikeyan K, Satish A, Krishnaswamy VR, Venugopal JR, Ramakrishna S. Recent advancements in nanotechnological strategies in selection, design and delivery of biomolecules for skin regeneration. Materials Science and Engineering: C. 2016;67:747-65.

20. Jalil WBF, Pentón-Madrigal A, Mello A, Carneiro FA, Soares RM, Baptista LS, et al. Low toxicity superparamagnetic magnetite nanoparticles: One-pot facile green synthesis for biological applications. Materials Science and Engineering: C. 2017;78:457-66.

21. Wang F, Li X, Li W, Bai H, Gao Y, Ma J, et al. Dextran coated Fe3O4 nanoparticles as a near-infrared laser-driven photothermal agent for efficient ablation of cancer cells in vitro and in vivo. Materials Science and Engineering: C. 2018;90:46-56.

22. Yang R-M, Fu C-P, Li N-N, Wang L, Xu X-D, Yang D-Y, et al. Glycosaminoglycan-targeted iron oxide nanoparticles for magnetic resonance imaging of liver carcinoma. Materials Science and Engineering: C. 2014;45:556-63.

23. Bishnoi M, Jain A, Hurkat P, Jain SK. Chondroitin sulphate: a focus on osteoarthritis. Glycoconjugate journal. 2016;33(5):693-705.

24. Fajardo AR, Guerry A, Britta EA, Nakamura CV, Muniz EC, Borsali R, et al. Sulfated glycosaminoglycan-based block copolymer: preparation of biocompatible chondroitin sulfate-b-poly (lactic acid) micelles. Biomacromolecules. 2014;15(7):2691-700.

25. da Cunha AL, de Oliveira LG, Maia LF, de Oliveira LFC, Michelacci YM, de Aguiar JAK. Pharmaceutical grade chondroitin sulfate: Structural analysis and identification of contaminants in different commercial preparations. Carbohyd Polym. 2015;134:300-8.

26. Mikami T, Kitagawa H. Biosynthesis and function of chondroitin sulfate. Biochimica et Biophysica Acta (BBA)-General Subjects. 2013;1830(10):4719-33.

27. Reginster J-Y, Gillot V, Bruyere O, Henrotin Y. Evidence of nutriceutical effectiveness in the treatment of osteoarthritis. Curr Rheumatol Rep. 2000;2(6):472-7.

28. du Souich P, García AG, Vergés J, Montell E. Immunomodulatory and anti‐inflammatory effects of chondroitin sulphate. Journal of cellular and molecular medicine. 2009;13(8a):1451-63.

29. Kubo M, Ando K, Mimura T, Matsusue Y, Mori K. Chondroitin sulfate for the treatment of hip and knee osteoarthritis: current status and future trends. Life sciences. 2009;85(13):477-83.

30. Muzzarelli RA, Greco F, Busilacchi A, Sollazzo V, Gigante A. Chitosan, hyaluronan and chondroitin sulfate in tissue engineering for cartilage regeneration: A review. Carbohyd Polym. 2012;89(3):723-39.

31. Lee C-T, Kung P-H, Lee Y-D. Preparation of poly (vinyl alcohol)-chondroitin sulfate hydrogel as matrices in tissue engineering. Carbohyd Polym. 2005;61(3):348-54.

32. Cheng K-M, Hung Y-W, Chen C-C, Liu C-C, Young J-J. Green synthesis of chondroitin sulfate-capped silver nanoparticles: characterization and surface modification. Carbohyd Polym. 2014;110:195-202.

33. Cho H-J, Oh J, Choo M-K, Ha J-I, Park Y, Maeng H-J. Chondroitin sulfate-capped gold nanoparticles for the oral delivery of insulin. International journal of biological macromolecules. 2014;63:15-20.

34. Aoyagi M, Sato H, Yagi K, Fukuda N, Nishimoto S. Redox reactions of nitrite ions on the surface of colloidal magnetite particles coated with chondroitin sulfate. Colloid & Polymer Science. 2001;279(1):46-52.

35. Guilherme MR, Reis AV, Alves BRV, Kunita MH, Rubira AF, Tambourgi EB. Smart hollow microspheres of chondroitin sulfate conjugates and magnetite nanoparticles for magnetic vector. Journal of Colloid and Interface Science. 2010;352(1):107-13.

36. Tóth IY, Illés E, Szekeres M, Tombácz E. Preparation and characterization of chondroitin‐sulfate‐A‐coated magnetite nanoparticles for biomedical applications. J Magn Magn Mater. 2015;380:168-74.

37. Liu M, Du H, Khan AR, Ji J, Yu A, Zhai G. Redox/enzyme sensitive chondroitin sulfate-based self-assembled nanoparticles loading docetaxel for the inhibition of metastasis and growth of melanoma. Carbohyd Polym. 2018;184:82-93.

38. Khalid I, Ahmad M, Usman Minhas M, Barkat K. Synthesis and evaluation of chondroitin sulfate based hydrogels of loxoprofen with adjustable properties as controlled release carriers. Carbohyd Polym. 2018;181:1169-79.

39. Kang YS, Risbud S, Rabolt JF, Stroeve P. Synthesis and Characterization of Nanometer-Size Fe3O4 and γ-Fe2O3 Particles. Chemistry of Materials. 1996;8(9):2209-11.

40. Santos JGM, Souza JR, Letti CJ, Soler MAG, Morais PC, Pereira-da-Silva MA, et al. Iron Oxide Nanostructured Electrodes for Detection of Copper(II) Ions. J Nanosci Nanotechno. 2014;14(9):6614-23.

41. Letti CJ, Paterno LG, Pereira-da-Silva MA, Morais PC, Soler MAG. The role of polymer films on the oxidation of magnetite nanoparticles. Journal of Solid State Chemistry. 2017;246:57-64.

42. Qu F, Morais PC. An oxide semiconductor nanoparticle in an aqueous medium: A surface charge density investigation. The Journal of Physical Chemistry B. 2000;104(22):5232-6.

43. Pereira LO, Longo JP, Azevedo RB. Laser irradiation did not increase the proliferation or the differentiation of stem cells from normal and inflamed dental pulp. Arch Oral Biol. 2012;57(8):1079-85.

44. Bacri J-C, Perzynski R, Salin D, Cabuil V, Massart R. Ionic ferrofluids: A crossing of chemistry and physics. J Magn Magn Mater. 1990;85(1–3):27-32.

45. da Silva SW, Melo TFO, Soler MAG, Lima ECD, da Silva AF, Morais PC. Stability of citrate-coated magnetite and cobalt-ferrite nanoparticles under laser irradiation: A Raman spectroscopy investigation. Ieee T Magn. 2003;39(5):2645-7.

46. Soler MG, Qu F. Raman Spectroscopy of Iron Oxide Nanoparticles. In: Kumar CSR, editor. Raman Spectroscopy for Nanomaterials Characterization: Springer Berlin Heidelberg; 2012. p. 379-416.

47. Mainreck N, Brézillon S, Sockalingum GD, Maquart F-X, Manfait M, Wegrowski Y. Rapid characterization of glycosaminoglycans using a combined approach by infrared and Raman microspectroscopies. Journal of Pharmaceutical Sciences. 2011;100(2):441-50.

48. Almodovar J, Place LW, Gogolski J, Erickson K, Kipper MJ. Layer-by-layer assembly of polysaccharide-based polyelectrolyte multilayers: a spectroscopic study of hydrophilicity, composition, and ion pairing. Biomacromolecules. 2011;12(7):2755-65.

49. Deacon GB, Phillips RJ. Relationships between the carbon-oxygen stretching frequencies of carboxylato complexes and the type of carboxylate coordination. Coordination Chemistry Reviews. 1980;33(3):227-50.

50. Eloiza SN, Emilia CDL, Maria AGS, Fabio RLS, Ricardo BA, Paulo CM. Evidence of iron (III) reduction in γ -Fe 2 O 3 nanoparticles due to meso-2,3-dimercaptosuccinic acid functionalization. Materials Research Express. 2014;1(1):016107.

51. Tulebayeva DZ, Kozlovskiy AL, Korolkov IV, Gorin YG, Kazantsev AV, Abylgazina L, et al. Modification of Fe 3 O 4 nanoparticles with carboranes. Materials Research Express. 2018;5(10):105011.

52. Franklin AD, Berkowitz AE. The Approach to Saturation in Dilute Ferromagnetics. Physical Review. 1953;89(6):1171.

53. Shaterabadi Z, Nabiyouni G, Soleymani M. High impact of in situ dextran coating on biocompatibility, stability and magnetic properties of iron oxide nanoparticles. Materials Science and Engineering: C. 2017;75:947-56.

54. Wei C, Xiaonan L, Wei W, Guangfu Y. Magnetic Fe 3 O 4 nanorings for protein adsorption and detection. Materials Research Express. 2018;5(12):125402.

55. Tung L, Kolesnichenko V, Caruntu D, Chou N, O'connor C, Spinu L. Magnetic properties of ultrafine cobalt ferrite particles. J Appl Phys. 2003;93(10):7486-8.

56. Shafi KV, Gedanken A, Prozorov R. Sonochemical preparation and characterization of nanosized amorphous Co–Ni alloy powders. Journal of Materials Chemistry. 1998;8(3):769-73.

57. Zou XH, Jiang YZ, Zhang GR, Jin HM, Hieu NTM, Ouyang HW. Specific interactions between human fibroblasts and particular chondroitin sulfate molecules for wound healing. Acta Biomaterialia. 2009;5(5):1588-95.

58. Luo M, Chen J, Li S, Sun H, Zhang Z, Fu Q, et al. Changes in the metabolism of chondroitin sulfate glycosaminoglycans in articular cartilage from patients with Kashin–Beck disease. Osteoarthritis and Cartilage. 2014;22(7):986-95.

59. Yamada S. Catabolism of chondroitin sulfate. Cellular and Molecular Biology Letters2015. p. 196.